



# Krypton Tagging Velocimetry (KTV) Investigation in the Caltech T5 Reflected-Shock Tunnel

D. Shekhtman\* M. A. Mustafa† N. J. Parziale‡

*Stevens Institute of Technology, Hoboken, NJ 07030, USA*

W. M. Yu§ J. M. Austin¶

*California Institute of Technology, Pasadena, CA 91125, USA*

Results are presented for a Krypton Tagging Velocimetry (KTV) investigation of the freestream flow of the T5 reflected shock tunnel at Caltech. This KTV scheme utilizes two-photon excitation at 216.67 nm with a pulsed dye laser, followed by re-excitation at 769.4547 nm with a continuous laser diode. Results are presented for experiments performed in 97% N<sub>2</sub>/3% Kr and 99% N<sub>2</sub>/1% Kr gas mixtures at a unit Reynolds number of approximately  $4 \times 10^6 \text{ m}^{-1}$  and a reservoir mass-specific enthalpy of approximately 5 MJ/kg. Agreement between the KTV derived velocity measurement and the computational results is excellent, within the uncertainty of the experiment.

## Nomenclature

$\lambda_{air}$	=	Transition wavelength measured in air, (nm)
$A_{ki}$	=	Einstein coefficient for transition from level $k$ to $i$ , ( $\text{s}^{-1}$ )
$E_i$	=	Energy of level $i$ , ( $\text{cm}^{-1}$ )
$M$	=	Mach number, (-)
$Re^{\text{unit}}$	=	Unit Reynolds number, ( $\text{m}^{-1}$ )
$P$	=	Pressure, (Pa)
$T$	=	Temperature, (K)
$\rho$	=	Density, ( $\text{kgm}^{-3}$ )
$h$	=	Specific enthalpy, ( $\text{MJ kg}^{-1}$ )
$t$	=	Time, (s)
$U$	=	Streamwise velocity, ( $\text{ms}^{-1}$ )
$x$	=	Streamwise coordinate, (m)
$r$	=	radial coordinate, (mm)

## Subscripts

$s$	=	Shock wave
$\infty$	=	Nozzle freestream
1	=	Region 1 (upstream of shock)
$R$	=	Nozzle reservoir

## I. Introduction

High-speed flow is characterized by complex phenomena such as shock waves, turbulence, and non-equilibrium thermochemistry. These phenomena and their interactions have implications for the fundamental behavior of high-speed flow, and consequently, design implications for high-speed vehicles. To study high-speed flows

\*Graduate Student, Mechanical Engineering, Castle Point on Hudson, Hoboken, New Jersey, 07030.

†Postdoctoral Researcher, Mechanical Engineering, Castle Point on Hudson, Hoboken, New Jersey, 07030.

‡Associate Professor, Mechanical Engineering, Castle Point on Hudson, Hoboken, New Jersey, 07030, AIAA Senior Member.

§PhD Candidate, Graduate Aerospace Laboratories, 1200 E. California Blvd, MC 105-50.

¶Professor of Aerospace, Graduate Aerospace Laboratories, 1200 E. California Blvd, MC 105-50, Associate Fellow AIAA

and optimize the design of high-speed vehicles, it is necessary to characterize performance in ground test; however, no single ground-test facility can recreate all high-speed flow conditions for free flight.<sup>1-3</sup>

One high-speed facility type is the impulse facility which aims to recreate free-flight enthalpy in ground test. Measurements in impulse facilities are notoriously difficult to make. Challenges include timing, frequency response, influence of the probe on the flow, harsh measurement environment, vibrational environment, and, in the case of particle-based techniques, particle injection. Non-intrusive optical diagnostics can address some of these challenges. In this work, we focus on velocity measurements.

There are two ubiquitous velocimetry techniques: Laser Doppler Velocimetry (LDV) and Particle Image Velocimetry (PIV).<sup>4</sup> These particle-based measurements rely on the assumption that the tracer particles travel identically with the flow. However, the particle response time can be inadequate in low-density flows with short time scales. Researchers have found that at low densities the Knudsen number of a particle can become large.<sup>5</sup> This represents a fundamental limitation of particle-based techniques because the slip condition at the particle surface culminates in reduced response time making critical quantities difficult to measure.<sup>6-8</sup>

Tagging velocimetry (TV) is an attractive alternative to particle-based techniques because TV is not limited by timing issues associated with tracer injection or reduced particle response at Knudsen and Reynolds numbers characteristic of high-speed wind tunnels. Methods of tagging velocimetry include KTV,<sup>9-18</sup> VENOM,<sup>19-23</sup> APART,<sup>24-26</sup> RELIEF,<sup>27-31</sup> FLEET,<sup>32,33</sup> STARFLEET,<sup>34</sup> PLEET,<sup>35</sup> argon,<sup>36</sup> iodine,<sup>37,38</sup> sodium,<sup>39</sup> acetone,<sup>40-42</sup> NH<sub>3</sub><sup>43</sup> and the hydroxyl group techniques,<sup>44-47</sup> among others.<sup>48-53</sup>

Researchers have applied various velocimetry techniques to impulse facilities. McIntosh<sup>54</sup> used spark tracer and magnetohydrodynamic methods to measure the velocity of the gas in the free stream of a high-enthalpy shock tunnel; the measurements appear to have large uncertainty with a somewhat complicated experimental setup. Wagner et al.<sup>55</sup> used PIV to measure the impulsively started flow over a cylinder in a shock tube. Haertig et al.<sup>56</sup> and Havermann et al.<sup>57</sup> use PIV to measure the flow of a cylinder and a jet in a shock tunnel at modest enthalpy. Parker et al.<sup>58</sup> used a line-of-sight-integrating method to measure freestream velocity via nitric oxide (NO) in the CUBRC LENS I facility. Danehy et al.<sup>59</sup> used NO as a tracer to measure shear flows in the T2 and T3 reflected-shock tunnels; those measurements used a mixture of approximately 97-99% N<sub>2</sub> and 1-3% O<sub>2</sub> in the driven section to “produce an amount of NO sufficient to produce good fluorescence but that would minimize the amount of the gases (O<sub>2</sub>, O, and NO) that are efficient quenchers.” de S. Matos et al.<sup>60</sup> made velocity measurements in unseeded hypersonic air flows in a reflected-shock tunnel at approximately 6 MJ/kg; that work presents a strategy where a reference image was taken before the test, which is not possible in some impulse facilities due to vibration.

In this work, we focus on applying Krypton Tagging Velocimetry (KTV) to measure a velocity profile in the freestream of the T5 Reflected-Shock Tunnel<sup>61</sup> at the California Institute of Technology. Preliminary experiments include two N<sub>2</sub> shots at 5 MJ/kg and a unit Reynolds number of approximately  $4 \times 10^6 \text{ m}^{-1}$ . We describe the experiment, the experimental results, and comparison to computation, and discuss future plans.

## II. Krypton Tagging Velocimetry

In this work, we focus on the use of Kr as a tracer for tagging velocimetry. The use of a metastable noble gas as a tagging velocimetry tracer was first suggested by Mills et al.<sup>62</sup> and Balla and Everheart.<sup>63</sup> To date, krypton tagging velocimetry (KTV) has been demonstrated by globally seeding high-speed N<sub>2</sub> flows with 1% Kr and air flows with 5% Kr. Applications include: 1) an underexpanded jet (first KTV demonstration);<sup>9</sup> 2) mean and fluctuating turbulent boundary-layer profiles in a Mach 2.7 flow;<sup>10</sup> 3) twenty simultaneous profiles over a 20 mm field-of-view of streamwise velocity and velocity fluctuations in a Mach 2.8 shock-wave/turbulent boundary-layer interaction;<sup>16</sup> and 4) the freestream of the large-scale AEDC Hypervelocity Tunnel 9 at Mach 10 and Mach 14.<sup>13</sup> In these experiments, the researchers used a pulsed dye-laser to perform the write step at 214.77 nm to form a write line and photosynthesize the metastable Kr tracer; after a prescribed delay, an additional pulsed dye-laser was used to re-excite the metastable Kr tracer to track displacement. Recently, simplified KTV schemes were developed and demonstrated in an underexpanded jet configuration<sup>15</sup> and in the flow following the incident shock in a shock tube.<sup>17</sup> These simplified schemes utilized either a dye-laser and a laser diode or a single dye laser to create the fluorescence lines.

In this work, we build upon the simplified schemes by utilizing a dye-laser and laser diode and demonstrate the use of two-photon excitation at 216.67 nm. This is in comparison to the 212.56 and 214.77 nm wavelengths used in previous KTV works. This change in two-photon wavelength to 216.67 nm is born out of the need to maximize the signal-to-noise ratio (SNR) of the fluorescence images. Details on the experimental and theoretical work justifying the use of 216.67 nm can be found in Shekhtman et al.<sup>64</sup>

Following the transitions in the energy level diagram in Figure 1 along with the relevant transition data in Table 1 (labeled as A, B, C), the KTV scheme is performed as follows:

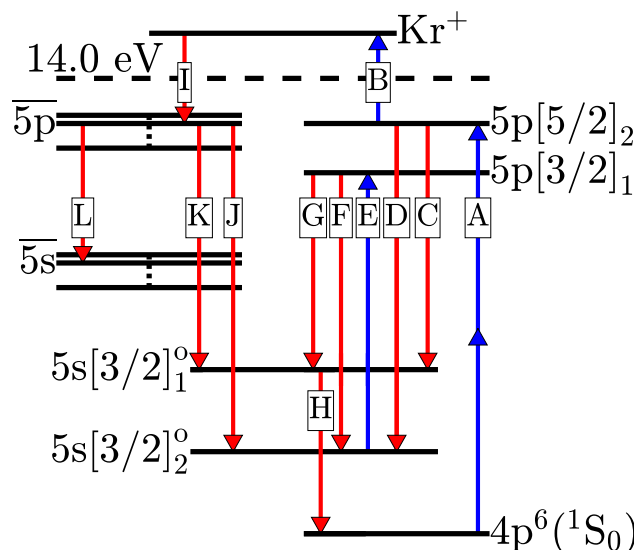


Figure 1: Energy diagram with Racah  $nl[K]_J$  notation. Blue lines indicate stimulated (laser induced) transitions and red lines indicate spontaneous transitions. States  $\bar{5}p$  and  $\bar{5}s$  represent the numerous 5p and 5s states that are created by the recombination process. Transitions J, K and L represent the numerous transitions in the 5p-5s band. 14.0 eV marks ionization limit of Kr. Transition details in Table 1.

1. **Write Step:** A pulsed tunable laser excites krypton atoms to form two tagged tracers, metastable Kr and Kr<sup>+</sup>, through (2+1) photoionization. Two-photon excitation of  $4p^6(^1S_0) \rightarrow 5p[5/2]_2$  (216.67 nm, transition A) and subsequent one-photon ionization<sup>65</sup> to Kr<sup>+</sup> (216.67 nm, transition B) occur. This is followed by transitions to metastable  $5p[5/2]_2 \rightarrow 5s[3/2]_2^o$  (transition D) and resonance states  $5p[5/2]_2 \rightarrow 5s[3/2]_1^o$  (transition C), as well as transitions (J, K and L) to states resulting from the recombination process,<sup>66,67</sup> I. The position of the write line is marked by gated imaging of the laser-induced-fluorescence (LIF) from these transitions (C, D, J, K, L), recorded with a camera positioned normal to the flow.
2. **Read Step:** After a prescribed delay, the displacement of the tagged metastable krypton and Kr<sup>+</sup> is recorded. An additional tunable laser excites  $5p[3/2]_1$  level by  $5s[3/2]_2^o \rightarrow 5p[3/2]_1$  transition (769.454 nm, E). This is followed by decay to metastable  $5p[3/2]_1 \rightarrow 5s[3/2]_1^o$  (829.81 nm, G) and resonance  $5p[3/2]_1 \rightarrow 5s[3/2]_2^o$  (769.454 nm, F) states. The position of the read line is marked by gated imaging of the LIF from transitions F and G, and the residual fluorescence from transitions J, K and L that result from the recombination process, I.

### III. Facility and Experimental Setup

All measurements were made in T5, the free-piston driven reflected-shock tunnel at the California Institute of Technology (Fig. 2). It is the fifth in a series of shock tunnels designed to simulate high-enthalpy, real gas effects on the aerodynamics of vehicles flying at hypervelocity speeds through the atmosphere. More information regarding the capabilities of T5 can be found in Hornung.<sup>61</sup>

An experiment in T5 is conducted as follows: a 120 kg aluminum piston is loaded into the compression tube/secondary reservoir junction. A secondary diaphragm (mylar, 127  $\mu$ m thick) is inserted at the nozzle throat at the end of the shock tube near the test section and a primary diaphragm (stainless steel, 7-

Table 1: Relevant NIST Atomic Spectra Database Lines Data, labels match Figure 1. Racah  $nl[K]_J$  notation. Transition I is not listed because it represents the recombination process. Entries in the J/K/L row represent ranges and order of magnitude estimates for transitions that involve excited Kr species in the 5p-5s band, as shown in Fig. 1.

Transition	$\lambda_{\text{air}}$ (nm)	Nature	$A_{ki}$ (1/s)	$E_i$ ( $\text{cm}^{-1}$ )	$E_k$ ( $\text{cm}^{-1}$ )	Lower Level	Upper Level
A	216.670	Two-Photon	(-)	0	92307.3786	$4s^2 4p^6, ^1S_0$	$5p[5/2]_2$
B	216.670	Single-Photon	(-)	92307.3786	112917.62	$5p[5/2]_2$	Kr+
C	877.675	Single-Photon	$2.2 \times 10^7$	80916.7680	92307.3786	$5s[3/2]_1$	$5p[5/2]_2$
D	810.436	Single-Photon	$8.9 \times 10^6$	79971.7417	92307.3786	$5s[3/2]_2$	$5p[5/2]_2$
E/F	769.454	Single-Photon	$4.3 \times 10^6$	79971.7417	92964.3943	$5s[3/2]_2$	$5p[3/2]_1$
G	829.811	Single-Photon	$2.9 \times 10^7$	80916.7680	92964.3943	$5s[3/2]_1$	$5p[3/2]_1$
H	123.584	Single-Photon	$3.0 \times 10^8$	0	80916.7680	$4s^2 4p^6, ^1S_0$	$5s[3/2]_1$
J/K/L	750-830	Single-Photon	$10^6 - 10^7$	80000.0000	90000.0000	$\bar{5}s$	$\bar{5}p$

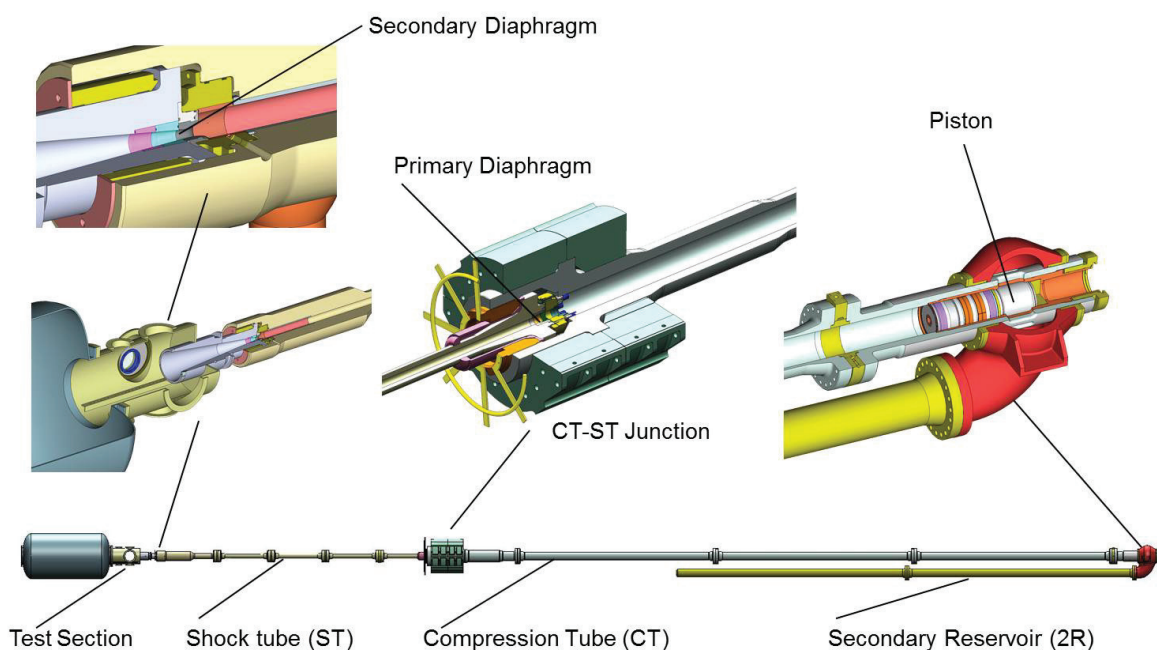


Figure 2: Schematic of the T5 reflected shock tunnel.

10 mm thick) is inserted at the compression tube/shock tube junction. The test section, shock tube, and compression tube are evacuated. The shock tube is filled with the test gas, the compression tube is filled with a He/Ar mixture to  $\approx 45$ -150 kPa and the secondary reservoir is filled with air to  $\approx 2$ -11 MPa. The air in the secondary reservoir is released, driving the piston into the compression tube. This piston motion adiabatically compresses the driver gas of the shock tunnel to the rupture pressure of the primary diaphragm ( $\approx 20$ -120 MPa). Following the primary diaphragm rupture, a shock wave propagates in the shock tube, is reflected off the end wall, breaking the secondary diaphragm and re-processing the test gas. The test gas is then at high temperature ( $\approx 2000$ -9000 K) and pressure ( $\approx 15$ -80 MPa) with negligible velocity and is then expanded through a converging-diverging contoured nozzle to hypersonic Mach number in the test section.

To calculate the run conditions, the initial shock tube pressure,  $P_1$ , measured incident shock speed  $U_s$ , and reservoir pressure  $P_R$  are used.  $P_1$  and  $U_s$  are used to evaluate the conditions in region 5, when the test gas has been processed by both the incident and reflected shocks. The thermodynamic state of the gas in region 5 is then isentropically changed to  $P_R$ . This accounts for the weak expansion or compression waves that are reflected between the contact surface and the shock tube end wall. These calculations were performed using Cantera<sup>68</sup> with the Shock and Detonation Toolbox.<sup>69</sup> The appropriate thermodynamic data are found

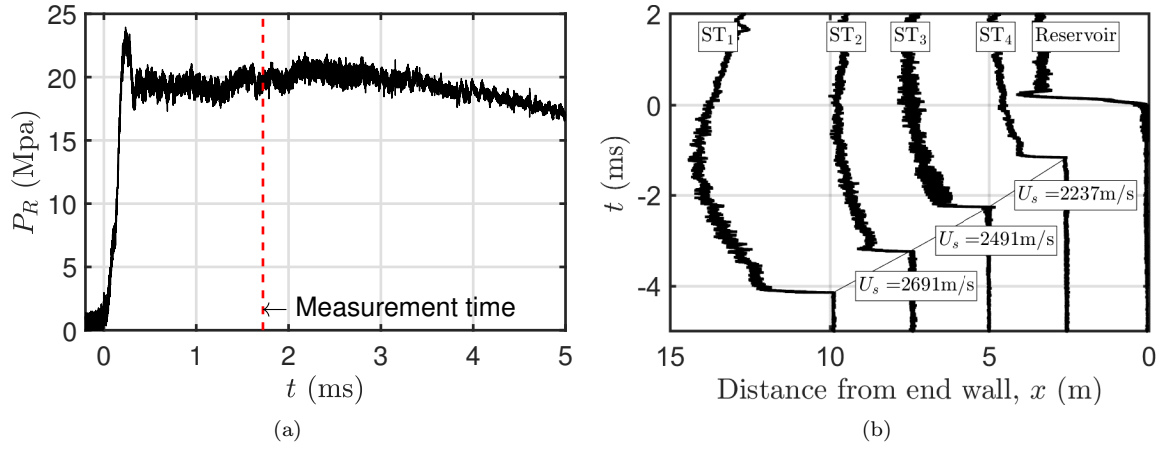


Figure 3: Shot 2909. a)  $P_R$  trace, red dashed line indicates time of write-laser pulse. b)  $x - t$  diagram. ST<sub>1-4</sub> indicate the four stations where shock speed is measured.

Table 2: Experimental Conditions.

Shot (-)	Gas (-)	$P_R$ (MPa)	$T_R$ (K)	$h_R$ (MJ/kg)	$P_\infty$ (kPa)	$T_\infty$ (K)	$\rho_\infty$ (kg m <sup>-3</sup> )	$M_\infty$ (-)	$U_\infty$ (ms <sup>-1</sup> )	$Re_\infty^{\text{unit}}$ (m <sup>-1</sup> )
2909	97% N <sub>2</sub> /3% Kr	19.9	4483	4.94	4.07	443.5	0.032	7.16	2983	$4.61 \times 10^6$
2910	99% N <sub>2</sub> /1% Kr	20.4	4489	5.18	4.44	460.9	0.033	7.02	3039	$4.03 \times 10^6$

in the literature.<sup>70,71</sup> Following the evaluation of the reservoir condition, the steady expansion through the contoured nozzle from the reservoir to the freestream is computed by the University of Minnesota Nozzle Code which modeled the flow as axisymmetric and solved reacting Navier-Stokes equations.<sup>72-75</sup>

In this work, two test gases were used, 97% N<sub>2</sub>/3% Kr and 99% N<sub>2</sub>/1% Kr. These Kr doped mixtures are intended to simulate N<sub>2</sub> flows with KTV. One shot was performed with each gas mixture at nominally same reservoir enthalpy of 5 MJ/kg. Fig. 3 shows the reservoir pressure trace and  $x - t$  diagram for shots 2909 (97% N<sub>2</sub>/3% Kr). The results for shot 2910 (99% N<sub>2</sub>/1% Kr) are nominally the same. The dashed red line indicates the time when the write laser was pulsed for the KTV measurement. In the  $x - t$  diagram, the pressure traces of the four stations in the shock tube and the reservoir are plotted at their spatial locations. The shock speed is calculated by dividing the transit distance by the transit time. The shock speed between station 4 and the reservoir transducer is not reported because the reservoir pressure tap is not designed for accurate time of arrival measurements. The shock speed between stations 3 and 4 is used for the thermochemical equilibrium calculations because it is estimated by  $x - t$  diagram that this location corresponds to the steady portion of the test gas slug.<sup>76</sup>

The write-laser system for this KTV scheme is a frequency-doubled Quanta Ray Pro-350 Nd:YAG laser and a frequency tripled Sirah PrecisionScan Dye Laser (DCM dye, DMSO solvent). A schematic of the optical setup is shown in Fig. 4. The Nd:YAG laser pumps the dye laser with 1000 mJ/pulse at a wavelength of 532 nm. The dye laser is tuned to output a 650.01 nm beam and frequency tripling (Sirah THU 205) of the dye-laser output results in a 216.67 nm beam, with 4 mJ energy entering the test section, 1350 MHz linewidth, and 7 ns pulsewidth at a repetition rate of 10 Hz. The write beam was focused into the test section with a 1000 mm focal-length, fused-silica lens. The beam fluence and spectral intensity at the waist were  $1.67 \times 10^3$  J/cm<sup>2</sup> and  $1.77 \times 10^2$  W/(cm<sup>2</sup> Hz), respectively. Additionally, we will present data with sufficient SNR 35 mm away from the focal point where the beam fluence and spectral intensity are quite a bit lower at 202.8 J/cm<sup>2</sup> and 21.5 W/(cm<sup>2</sup> Hz), respectively.

The laser diode used in this work is a Topica TA Pro Laser diode. It provided the 769.45470 nm laser excitation of metastable Kr ( $4p^5(2P_{3/2}^o 5s^2[3/2]_2^o)$ ) with a nominal, output laser power of 2.6 W. Although not as simple as a single-laser setup, the laser diode is much easier to manage than a second pulsed dye

laser, as was used previously. A feedback loop for wavelength reference tracking was implemented to lock the diode on the desired wavelength. The Topica TA Pro Laser diode was treated as the plant. The Topica DCL Pro Controller was the actuator, sending piezoelectric control voltages into the laser diode. The DCL Pro was set on Analog Remote Control PC for external piezoelectric control. Of the three diode parameters—temperature, current, and piezoelectric voltage—that the Topica DCL Pro Controller regulated, piezoelectric control was selected to minimize the response time, the effect of hysteresis, and the effect of changing operational conditions. The gain on the DCL Pro was set to 8. The Wavelength Meter WS7-4150 measured the wavelength in air of the laser diode. This measurement served as the feedback signal for the control law stored on the wavemeter software. The proportional-integral (PI) control law was

$$u(t) = k_p (\lambda_{diode} - \lambda_{des}) + \frac{k_i}{w_i} \int_0^t (\lambda_{diode} - \lambda_{des}) dt, \quad (1)$$

where  $k_p$  is the control gain;  $k_i$  is the integral gain;  $t_a$  is the weight on the integral gain controlling sensitivity;  $\lambda_{diode}$  is the laser diode wavelength;  $\lambda_{des}$  is the desired wavelength to be tracked;  $t$  is time. The control parameters for the PI controller are shown in Table 3, which were experimentally obtained. Note that the derivative gain  $k_d$  is set to zero; constant timestep  $dt$  is checked; and the sensitivity was set either to 5V/10pm or 5V/1pm for sensitivity. The exposure time was minimized to 90-100 ms to maximize the sampling rate of the wavemeter. The low sampling rate required a large weight  $t_a = 10$  on the integral controller to ensure stability. In order to prevent saturation of the piezoelectric voltage (actuator saturation), manual tuning of the diode diffraction grating via a 2.5 mm Allen key was used to bring the diode within  $\pm 0.02$  nm from the desired operating wavelength.

Table 3: Control Parameters for PI Controller.

Parameter	Value
$k_p$	0.5-0.6
$k_i$	0.5-0.6
$w_i$	10

The intensified CCD camera used for all experiments is a Princeton Instruments PIMAX-4 (PM4-1024i-HR-FG-18-P46-CM) with an AF-S NIKKOR 200mm f/2G ED-VR-II prime lens positioned approximately 18 in from the write/read location. The camera gate opens twice: once for 5 ns immediately following the write-laser pulse and again at a prescribed delay time of 500 ns for 50 ns to capture the transitions from the read step. The inherent luminosity of the flow in the T5 tunnel has the deleterious effect of obscuring the fluorescence signal. To mitigate this, three 800 nm high pass and two 850 nm low pass filters were placed in front of the camera. The filters also decrease the KTV signal; however, this does not outweigh the benefit of reducing the effect of the flow luminosity.

A technical issue associated with using laser diagnostics in impulse facilities is timing. In this work, the lasers need to be maintained at operating temperature by being continuously pulsed at 10 Hz while also pulsing at a set instant for the measurement. Here, the probe time was chosen to be 1.5 ms after  $P_R$  has been established, see red dashed line in Fig. 3. The delay of 1.5 ms accounts for the nozzle start-up and flow establishment time in the test section.

Fig. 4 shows the optical setup and timing circuit associated with these experiments. The timing is a three-step process. First, pulse the laser continuously at 10 Hz to maintain the operating temperature. Second, pause the laser system when the tunnel starts, and third, trigger a single laser pulse at the desired time to make the measurement. The pause is necessary as otherwise the measurement pulse could occur at a rate higher than 10 Hz, which is undesirable. The steps are detailed below, following the schematic in Fig. 4:

1. The pump laser is set up to operate at 10 Hz. This pulse rate is controlled by a pulse delay generator (PDG 1 in Fig. 4). PDG 1 is triggered by the signal from an amplifier/signal comparator, Amp 3. The output of Amp 3 is the signal from PDG 2 minus the signal from Amp 2. At this stage, the output of Amp 2 is 0 V. Therefore, the output of Amp 3 is the same as that of PDG 2. PDG 2 is triggered at a continuous 10 Hz from the function generator.



## IV. Results

In this section the results for the experiments in  $N_2$  are shown. Corresponding flow conditions are listed in tables 2. To process the KTV exposures, the line centers were found in the following way:

- 1) Crop the image to an appropriate field of view.
- 2) Apply a two-dimensional Wiener adaptive-noise removal filter.
- 3) Convert the images to double precision numbers and normalize the intensity to fall in the range of 0-1.
- 4) Apply the Gaussian peak finding algorithm from O’Haver<sup>77</sup> to find the line centers for the top row using the read lines in the top row of each image as a first guess.
- 5) Proceeding from the top-down, apply the Gaussian peak finding algorithm from O’Haver<sup>77</sup> to find the line centers for each row using the line center location immediately above as the guess.

Error bars for the KTV measurements are calculated in the same fashion as Zahradka et al.<sup>10</sup> as

$$\tilde{U}_{\text{KTV}} = \left[ \left( \tilde{\Delta x} \frac{\partial U}{\partial \Delta x} \right)^2 + \left( \tilde{\Delta t} \frac{\partial U}{\partial \Delta t} \right)^2 + \left( v'_{RMS} \frac{\partial U}{\partial y} \Delta t \right)^2 \right]^{\frac{1}{2}}, \quad (2)$$

where uncertainty estimates of a variable are indicated with a tilde. The uncertainty in the measured displacement distance,  $\tilde{\Delta x}$ , of the metastable tracer is estimated as the 95% confidence bound on the write and read locations from the Gaussian fits,  $\approx 10$  microns. The uncertainty in time,  $\tilde{\Delta t}$ , is estimated to be the camera gate width, 50 ns, causing fluorescence blurring.<sup>78</sup> The third term in Eq. 2 is uncertainty in streamwise velocity due to wall-normal fluctuations in the  $xy$ -plane,<sup>78,79</sup> where  $v'_{RMS}$  is estimated as the mean of the wall-normal velocity at the nozzle exit,  $\approx 40 \text{ ms}^{-1}$ .

The results for shots 2909 and 2910 are shown in Figs. 5 and 6. For each experiment, the plot on the left is the superposition of the write and read KTV images on which the Gaussian fits (in red) are superimposed. The plot on the right shows the derived KTV velocity profile in blue, the uncertainty estimate as black bars, and the computational results in red. The field of view of the KTV measurements is 40 mm and the uncertainty is estimated as 10% of the freestream value.

There is good agreement between the computational results and the KTV derived velocity, which brings confidence in the ability to use KTV for test and evaluation. There is no apparent flow luminosity in the raw KTV images, the result of a relatively low enthalpy and the use of filters. The SNR in shot 2910 is lower, as expected from a lower concentration of Kr.

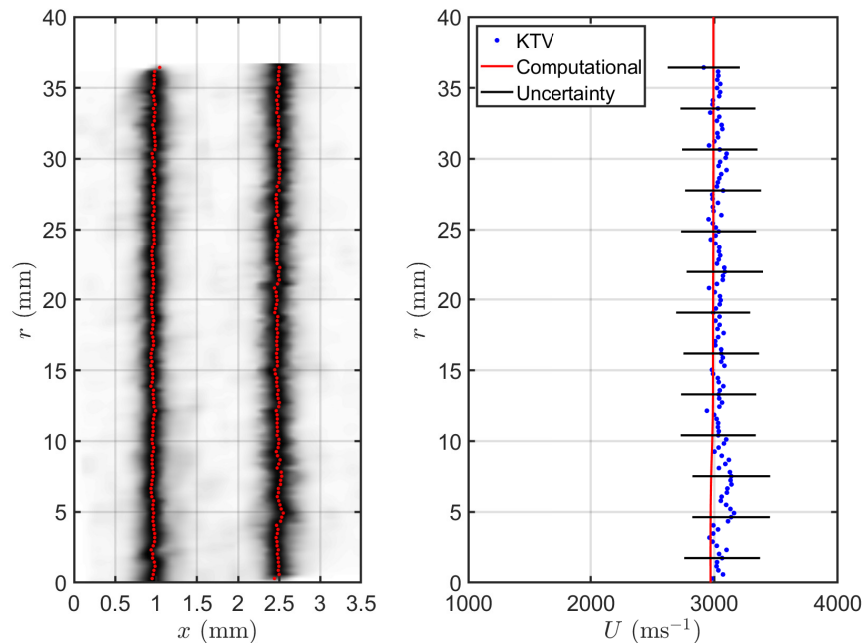


Figure 5: Shot 2909. *Left*: Superposition of raw write and read KTV images (inverted Scale). *Right*: KTV obtained velocity profile in blue, error bars in black, and computational results in red.

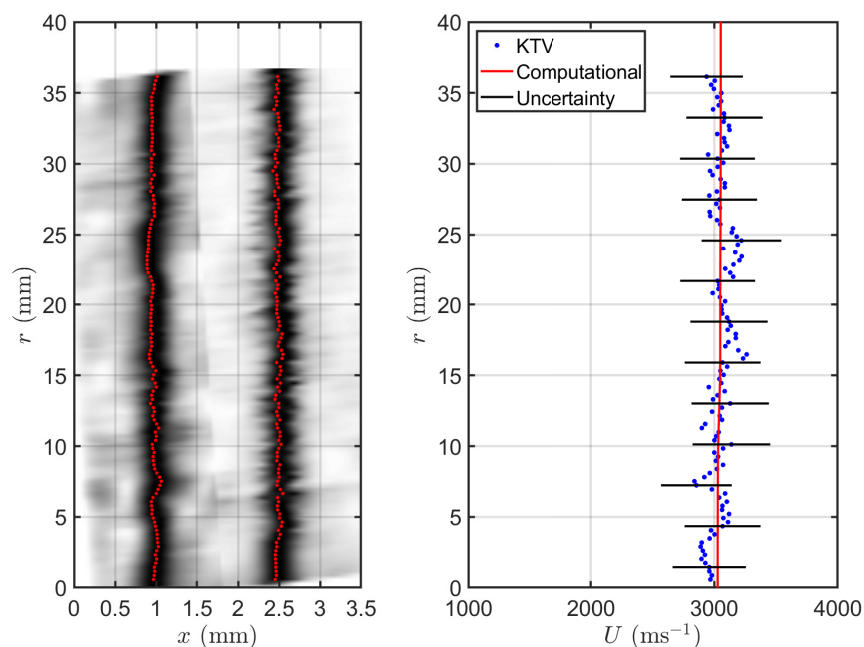


Figure 6: Shot 2910. *Left*: Superposition of raw write and read KTV images (inverted Scale). *Right*: KTV obtained velocity profile in blue, error bars in black, and computational results in red.

## V. Conclusions

KTV was applied to a high-enthalpy impulse facility, the T5 reflected shock tunnel at Caltech. Velocity measurements were made in the freestream at  $M_\infty \approx 7$  and  $Re_\infty^{\text{unit}} \approx 4 \times 10^6$ . The results from the KTV measurements are in good agreement with the DPLR Nozzle code results.

A new variation of KTV was demonstrated, which uses two-photon excitation at 216.67 nm, as opposed to the 212.56 and 214.77 nm use in previous works. This change in wavelength was experimentally determined to provide the highest SNR when used with a laser diode.

Two gas mixtures were used, 97%  $\text{N}_2$ /3% Kr and 99%  $\text{N}_2$ /1% Kr at a reservoir enthalpy of  $\approx 5$  MJ/kg. A new timing circuit was developed to maintain the laser system at operating temperature and also allow for control over the measurement time.

Future work in T5 includes the use of a 75%  $\text{N}_2$ /20%  $\text{O}_2$ /5% Kr gas mixture to simulate air, higher enthalpy shots, and making measurements over a test article such as a cone or double wedge. We anticipate that with higher enthalpies and pressures, flow luminosity and low SNR will present a challenge and/or possible limitations.

## Acknowledgments

Mustafa and Parziale were supported by AFOSR Young Investigator Program Grant FA9550-16-1-0262 and AFOSR Grant FA9550-18-1-0403; equipment for this work was supported by AFOSR DURIP Grants FA9550-15-1-0325 and FA9550-19-1-0182. Support was provided by U.S. Air Force Small Business Innovation Research grants FA9101-17-P-0094 and FA2487-19-C-0013. Shekhtman was supported by the Stevens Institute of Technology Provost Fellowship and the ONR Young Investigator Research Program Grant N00014-20-1-2549.

We would like to acknowledge Hans Hornung of Caltech for providing valuable advice regarding all aspects of the project. Additionally, we would like to thank Bahram Valiferdowsi, also of Caltech, for operating the tunnel and assisting with the experimental setup.

## References

- <sup>1</sup>Hornung, H. G., “Experimental Hypervelocity Flow Simulation, Needs, Achievements and Limitations,” *Proceedings of the First Pacific International Conference on Aerospace Science and Technology*, Taiwan, 1993.
- <sup>2</sup>Lu, F. K. and Marren, D. E., *Advanced Hypersonic Test Facilities*, AIAA, 2002. doi: [10.2514/4.866678](https://doi.org/10.2514/4.866678).
- <sup>3</sup>Schneider, S. P., “Development of Hypersonic Quiet Tunnels,” *Journal of Spacecraft and Rockets*, Vol. 45, No. 4, 2008, pp. 641–664. doi: [10.2514/1.34489](https://doi.org/10.2514/1.34489).
- <sup>4</sup>Tropea, C., Yarin, A. L., and Foss, J. F., *Springer Handbook of Experimental Fluid Mechanics*, Springer, 2007.
- <sup>5</sup>Loth, E., “Compressibility and Rarefaction Effects on Drag of a Spherical Particle,” *AIAA Journal*, Vol. 46, No. 9, 2008, pp. 2219–2228. doi: [10.2514/1.28943](https://doi.org/10.2514/1.28943).
- <sup>6</sup>Lowe, K. T., Byun, G., and Simpson, R. L., “The Effect of Particle Lag on Supersonic Turbulent Boundary Layer Statistics,” *Proceedings of AIAA SciTech 2014*, AIAA-2014-0233, National Harbor, Maryland, 2014. doi: [10.2514/6.2014-0233](https://doi.org/10.2514/6.2014-0233).
- <sup>7</sup>Williams, O. J. H., Nguyen, T., Schreyer, A.-M., and Smits, A. J., “Particle response analysis for particle image velocimetry in supersonic flows,” *Physics of Fluids*, Vol. 27, No. 7, 2015, pp. 076101. doi: [10.1063/1.4922865](https://doi.org/10.1063/1.4922865).
- <sup>8</sup>Brooks, J. M., Gupta, A. K., Smith, M. S., and Marineau, E. C., “Particle image velocimetry measurements of Mach 3 turbulent boundary layers at low Reynolds numbers,” *Experiments in Fluids*, Vol. 59, 2018, pp. 83. doi: [10.1007/s00348-018-2536-x](https://doi.org/10.1007/s00348-018-2536-x).
- <sup>9</sup>Parziale, N. J., Smith, M. S., and Marineau, E. C., “Krypton tagging velocimetry of an underexpanded jet,” *Applied Optics*, Vol. 54, No. 16, 2015, pp. 5094–5101. doi: [10.1364/AO.54.005094](https://doi.org/10.1364/AO.54.005094).
- <sup>10</sup>Zahradka, D., Parziale, N. J., Smith, M. S., and Marineau, E. C., “Krypton tagging velocimetry in a turbulent Mach 2.7 boundary layer,” *Experiments in Fluids*, Vol. 57, 2016, pp. 62. doi: [10.1007/s00348-016-2148-2](https://doi.org/10.1007/s00348-016-2148-2).
- <sup>11</sup>Mustafa, M. A., Hunt, M. B., Parziale, N. J., Smith, M. S., and Marineau, E. C., “Krypton Tagging Velocimetry (KTV) Investigation of Shock-Wave/Turbulent Boundary-Layer Interaction,” *Proceedings of AIAA SciTech 2017*, AIAA-2017-0025, Grapevine, Texas, 9-13 January 2017. doi: [10.2514/6.2017-0025](https://doi.org/10.2514/6.2017-0025).
- <sup>12</sup>Mustafa, M. A., , and Parziale, N. J., “Krypton Tagging Velocimetry in the Stevens Shock Tube,” *Proceedings of 33rd AIAA Aerodynamic Measurement Technology and Ground Testing Conference*, AIAA-2017-3897, Denver, Colorado, 5-9 June 2017. doi: [10.2514/6.2017-3897](https://doi.org/10.2514/6.2017-3897).
- <sup>13</sup>Mustafa, M. A., Parziale, N. J., Smith, M. S., and Marineau, E. C., “Nonintrusive Freestream Velocity Measurement in a Large-Scale Hypersonic Wind Tunnel,” *AIAA Journal*, Vol. 55, No. 10, 2017, pp. 3611–3616. doi: [10.2514/1.J056177](https://doi.org/10.2514/1.J056177).
- <sup>14</sup>Mustafa, M. A., Parziale, N. J., Smith, M. S., and Marineau, E. C., “Two-Dimensional Krypton Tagging Velocimetry (KTV-2D) Investigation of Shock-Wave/Turbulent Boundary-Layer Interaction,” *Proceedings of AIAA SciTech 2018*, AIAA-2018-1771, Kissimmee, Florida, 8-12 January 2018. doi: [10.2514/6.2018-1771](https://doi.org/10.2514/6.2018-1771).
- <sup>15</sup>Mustafa, M. A. and Parziale, N. J., “Simplified read schemes for krypton tagging velocimetry in N<sub>2</sub> and air,” *Optics Letters*, Vol. 43, No. 12, 2018, pp. 2909–2912. doi: [10.1364/OL.43.002909](https://doi.org/10.1364/OL.43.002909).
- <sup>16</sup>Mustafa, M. A., Parziale, N. J., Smith, M. S., and Marineau, E. C., “Amplification and structure of streamwise-velocity fluctuations in compression-corner shock-wave/turbulent boundary-layer interactions,” *Journal of Fluid Mechanics*, Vol. 863, 2019, pp. 1091–1122. doi: [10.1017/jfm.2018.1029](https://doi.org/10.1017/jfm.2018.1029).
- <sup>17</sup>Mustafa, M. A., Shekhtman, D., and Parziale, N. J., “Single-Laser Krypton Tagging Velocimetry Investigation of Supersonic Air and N<sub>2</sub> Boundary-Layer Flows over a Hollow Cylinder in a Shock Tube,” *Physical Review Applied*, Vol. 11, No. 6, 2019, pp. 064013. doi: [10.1103/PhysRevApplied.11.064013](https://doi.org/10.1103/PhysRevApplied.11.064013).
- <sup>18</sup>Shekhtman, D., Mustafa, M. A., and Parziale, N. J., “Two-photon cross-section calculations for krypton in the 190-220 nm range,” *Applied Optics*, Vol. 59, No. 34, 2020, pp. 10826–10837. doi: [10.1364/AO.410806](https://doi.org/10.1364/AO.410806).
- <sup>19</sup>Hsu, A. G., Srinivasan, R., Bowersox, R. D. W., and North, S. W., “Molecular Tagging Using Vibrationally Excited Nitric Oxide in an Underexpanded Jet Flowfield,” *AIAA Journal*, Vol. 47, No. 11, 2009, pp. 2597–2604. doi: [10.2514/1.39998](https://doi.org/10.2514/1.39998).
- <sup>20</sup>Hsu, A. G., Srinivasan, R., Bowersox, R. D. W., and North, S. W., “Two-component molecular tagging velocimetry utilizing NO fluorescence lifetime and NO<sub>2</sub> photodissociation techniques in an underexpanded jet flowfield,” *Applied Optics*, Vol. 48, No. 22, 2009, pp. 4414–4423. doi: [10.1364/AO.48.004414](https://doi.org/10.1364/AO.48.004414).
- <sup>21</sup>Sánchez-González, R., Srinivasan, R., Bowersox, R. D. W., and North, S. W., “Simultaneous velocity and temperature measurements in gaseous flow fields using the VENOM technique,” *Optics Letters*, Vol. 36, No. 2, 2011, pp. 196–198. doi: [10.1364/OL.36.000196](https://doi.org/10.1364/OL.36.000196).
- <sup>22</sup>Sánchez-González, R., Bowersox, R. D. W., and North, S. W., “Simultaneous velocity and temperature measurements in gaseous flowfields using the vibrationally excited nitric oxide monitoring technique: a comprehensive study,” *Applied Optics*, Vol. 51, No. 9, 2012, pp. 1216–1228. doi: [10.1364/AO.51.001216](https://doi.org/10.1364/AO.51.001216).
- <sup>23</sup>Sánchez-González, R., Bowersox, R. D. W., and North, S. W., “Vibrationally excited NO tagging by NO(A<sup>2</sup>Σ<sup>+</sup>) fluorescence and quenching for simultaneous velocimetry and thermometry in gaseous flows,” *Optics Letters*, Vol. 39, No. 9, 2014, pp. 2771–2774. doi: [10.1364/OL.39.002771](https://doi.org/10.1364/OL.39.002771).
- <sup>24</sup>Dam, N., Klein-Douwel, R. J. H., Sijtsema, N. M., and ter Meulen, J. J., “Nitric oxide flow tagging in unseeded air,” *Optics Letters*, Vol. 26, No. 1, 2001, pp. 36–38. doi: [10.1364/OL.26.000036](https://doi.org/10.1364/OL.26.000036).
- <sup>25</sup>Sijtsema, N. M., Dam, N. J., Klein-Douwel, R. J. H., and ter Meulen, J. J., “Air Photolysis and Recombination Tracking: A New Molecular Tagging Velocimetry Scheme,” *AIAA Journal*, Vol. 40, No. 6, 2002, pp. 1061–1064. doi: [10.2514/2.1788](https://doi.org/10.2514/2.1788).
- <sup>26</sup>Van der Laan, W. P. N., Tolboom, R. A. L., Dam, N. J., and ter Meulen, J. J., “Molecular tagging velocimetry in the wake of an object in supersonic flow,” *Experiments in Fluids*, Vol. 34, No. 4, 2003, pp. 531–534. doi: [10.1007/s00348-003-0593-1](https://doi.org/10.1007/s00348-003-0593-1).

- <sup>27</sup>Miles, R., Cohen, C., Connors, J., Howard, P., Huang, S., Markovitz, E., and Russell, G., "Velocity measurements by vibrational tagging and fluorescent probing of oxygen," *Optics Letters*, Vol. 12, No. 11, 1987, pp. 861–863. doi: [10.1364/OL.12.000861](https://doi.org/10.1364/OL.12.000861).
- <sup>28</sup>Miles, R., Connors, J., Markovitz, E., Howard, P., and Roth, G., "Instantaneous profiles and turbulence statistics of supersonic free shear layers by Raman excitation plus laser-induced electronic fluorescence (RELIEF) velocity tagging of oxygen," *Experiments in Fluids*, Vol. 8, No. 1-2, 1989, pp. 17–24. doi: [10.1007/BF00203060](https://doi.org/10.1007/BF00203060).
- <sup>29</sup>Miles, R. B., Zhou, D., Zhang, B., and Lempert, W. R., "Fundamental Turbulence Measurements by RELIEF Flow Tagging," *AIAA Journal*, Vol. 31, No. 3, 1993, pp. 447–452. doi: [10.2514/3.11350](https://doi.org/10.2514/3.11350).
- <sup>30</sup>Miles, R. B. and Lempert, W. R., "Quantitative Flow Visualization in Unseeded Flows," *Annual Review of Fluid Mechanics*, Vol. 29, No. 1, 1997, pp. 285–326. doi: [10.1146/annurev.fluid.29.1.285](https://doi.org/10.1146/annurev.fluid.29.1.285).
- <sup>31</sup>Miles, R. B., Grinstead, J., Kohl, R. H., and Diskin, G., "The RELIEF flow tagging technique and its application in engine testing facilities and for helium-air mixing studies," *Measurement Science and Technology*, Vol. 11, No. 9, 2000, pp. 1272–1281. doi: [10.1088/0957-0233/11/9/304](https://doi.org/10.1088/0957-0233/11/9/304).
- <sup>32</sup>Michael, J. B., Edwards, M. R., Dogariu, A., and Miles, R. B., "Femtosecond laser electronic excitation tagging for quantitative velocity imaging in air," *Applied Optics*, Vol. 50, No. 26, 2011, pp. 5158–5162. doi: [10.1364/AO.50.005158](https://doi.org/10.1364/AO.50.005158).
- <sup>33</sup>Edwards, M. R., Dogariu, A., and Miles, R. B., "Simultaneous Temperature and Velocity Measurements in Air with Femtosecond Laser Tagging," *AIAA Journal*, Vol. 53, No. 8, 2015, pp. 2280–2288. doi: [10.2514/1.J053685](https://doi.org/10.2514/1.J053685).
- <sup>34</sup>Jiang, N., Halls, B. R., Stauffer, H. U., Danehy, P. M., Gord, J. R., and Roy, S., "Selective two-photon absorptive resonance femtosecond-laser electronic-excitation tagging velocimetry," *Optics Letters*, Vol. 41, No. 10, 2016, pp. 2225–2228. doi: [10.1364/OL.41.002225](https://doi.org/10.1364/OL.41.002225).
- <sup>35</sup>Jiang, N., Mance, J. G., Slipchenko, M. N., Felver, J. J., Stauffer, H. U., Yi, T., Danehy, P. M., and Roy, S., "Seedless velocimetry at 100 kHz with picosecond-laser electronic-excitation tagging," *Optics Letters*, Vol. 42, No. 2, 2017, pp. 239–242. doi: [10.1364/OL.42.000239](https://doi.org/10.1364/OL.42.000239).
- <sup>36</sup>Mills, J. L., *Investigation of Multi-Photon Excitation in Argon with Applications in Hypersonic Flow Diagnostics*, Ph.D. thesis, Old Dominion University, 2016.
- <sup>37</sup>McDaniel, J. C., Hiller, B., and Hanson, R. K., "Simultaneous multiple-point velocity measurements using laser-induced iodine fluorescence," *Optics Letters*, Vol. 8, No. 1, 1983, pp. 51–53. doi: [10.1364/OL.8.000051](https://doi.org/10.1364/OL.8.000051).
- <sup>38</sup>Balla, R. J., "Iodine Tagging Velocimetry in a Mach 10 Wake," *AIAA Journal*, Vol. 51, No. 7, 2013, pp. 1–3. doi: [10.2514/1.J052416](https://doi.org/10.2514/1.J052416).
- <sup>39</sup>Barker, P., Bishop, A., and Rubinsztein-Dunlop, H., "Supersonic velocimetry in a shock tube using laser enhanced ionisation and planar laser induced fluorescence," *Applied Physics B*, Vol. 64, No. 3, 1997, pp. 369–376. doi: [10.1007/s003400050186](https://doi.org/10.1007/s003400050186).
- <sup>40</sup>Lempert, W. R., Jiang, N., Sethuram, S., and Samimy, M., "Molecular Tagging Velocimetry Measurements in Supersonic Microjets," *AIAA Journal*, Vol. 40, No. 6, 2002, pp. 1065–1070. doi: [10.2514/2.1789](https://doi.org/10.2514/2.1789).
- <sup>41</sup>Lempert, W. R., Boehm, M., Jiang, N., Gimelshein, S., and Levin, D., "Comparison of molecular tagging velocimetry data and direct simulation Monte Carlo simulations in supersonic micro jet flows," *Experiments in Fluids*, Vol. 34, No. 3, 2003, pp. 403–411. doi: [10.1007/s00348-002-0576-7](https://doi.org/10.1007/s00348-002-0576-7).
- <sup>42</sup>Handa, T., Mii, K., Sakurai, T., Imamura, K., Mizuta, S., and Ando, Y., "Study on supersonic rectangular microjets using molecular tagging velocimetry," *Experiments in Fluids*, Vol. 55, No. 5, 2014, pp. 1–9. doi: [10.1007/s00348-014-1725-5](https://doi.org/10.1007/s00348-014-1725-5).
- <sup>43</sup>Zhang, S., Yu, X., Yan, H., Huang, H., and Liu, H., "Molecular tagging velocimetry of NH fluorescence in a high-enthalpy rarefied gas flow," *Applied Physics B*, Vol. 123, No. 4, 2017, pp. 122. doi: [10.1007/s00340-017-6703-1](https://doi.org/10.1007/s00340-017-6703-1).
- <sup>44</sup>Boedeker, L. R., "Velocity measurement by H<sub>2</sub>O photolysis and laser-induced fluorescence of OH," *Optics Letters*, Vol. 14, No. 10, 1989, pp. 473–475. doi: [10.1364/OL.14.000473](https://doi.org/10.1364/OL.14.000473).
- <sup>45</sup>Wehrmeyer, J. A., Ribarov, L. A., Oguss, D. A., and Pitz, R. W., "Flame Flow Tagging Velocimetry with 193-nm H<sub>2</sub>O Photodissociation," *Applied Optics*, Vol. 38, No. 33, 1999, pp. 6912–6917. doi: [10.1364/AO.38.006912](https://doi.org/10.1364/AO.38.006912).
- <sup>46</sup>Pitz, R. W., Lahr, M. D., Douglas, Z. W., Wehrmeyer, J. A., Hu, S., Carter, C. D., Hsu, K.-Y., Lum, C., and Koochesfahani, M. M., "Hydroxyl tagging velocimetry in a supersonic flow over a cavity," *Applied Optics*, Vol. 44, No. 31, 2005, pp. 6692–6700. doi: [10.1364/AO.44.006692](https://doi.org/10.1364/AO.44.006692).
- <sup>47</sup>André, M. A., Bardet, P. M., Burns, R. A., and Danehy, P. M., "Characterization of hydroxyl tagging velocimetry for low-speed flows," *Measurement Science and Technology*, Vol. 28, No. 8, 2017, pp. 085202. doi: [10.1088/1361-6501/aa7ac8](https://doi.org/10.1088/1361-6501/aa7ac8).
- <sup>48</sup>Hiller, B., Booman, R. A., Hassa, C., and Hanson, R. K., "Velocity visualization in gas flows using laser-induced phosphorescence of biacetyl," *Review of Scientific Instruments*, Vol. 55, No. 12, 1984, pp. 1964–1967. doi: [10.1063/1.1137687](https://doi.org/10.1063/1.1137687).
- <sup>49</sup>Gendrich, C. P. and Koochesfahani, M. M., "A spatial correlation technique for estimating velocity fields using molecular tagging velocimetry (MTV)," *Experiments in Fluids*, Vol. 22, No. 1, 1996, pp. 67–77. doi: [10.1007/BF01893307](https://doi.org/10.1007/BF01893307).
- <sup>50</sup>Gendrich, C. P., Koochesfahani, M. M., and Nocera, D. G., "Molecular tagging velocimetry and other novel applications of a new phosphorescent supramolecule," *Experiments in Fluids*, Vol. 23, No. 5, 1997, pp. 361–372. doi: [10.1007/s003480050123](https://doi.org/10.1007/s003480050123).
- <sup>51</sup>Stier, B. and Koochesfahani, M. M., "Molecular tagging velocimetry (MTV) measurements in gas phase flows," *Experiments in Fluids*, Vol. 26, No. 4, 1999, pp. 297–304. doi: [10.1007/s003480050292](https://doi.org/10.1007/s003480050292).
- <sup>52</sup>Ribarov, L. A., Wehrmeyer, J. A., Batliwala, F., Pitz, R. W., and DeBarber, P. A., "Ozone Tagging Velocimetry Using Narrowband Excimer Lasers," *AIAA Journal*, Vol. 37, No. 6, 1999, pp. 708–714. doi: [10.2514/2.799](https://doi.org/10.2514/2.799).
- <sup>53</sup>André, M. A., Burns, R. A., Danehy, P. M., Cadell, S. R., Woods, B. G., and Bardet, P. M., "Development of N<sub>2</sub>O-MTV for low-speed flow and in-situ deployment to an integral effect test facility," *Experiments in Fluids*, Vol. 59, No. 1, 2018, pp. 14. doi: [10.1007/s00348-017-2470-3](https://doi.org/10.1007/s00348-017-2470-3).

- <sup>54</sup>McIntosh, M. K., “Free Stream Velocity Measurements in a High Enthalpy Shock Tunnel,” *The Physics of Fluids*, Vol. 14, No. 6, 1971, pp. 1100–1102. doi: [10.1063/1.1693570](https://doi.org/10.1063/1.1693570).
- <sup>55</sup>Wagner, J. L., DeMauro, E. P., Casper, K. M., Beresh, S. J., Lynch, K. P., and Pruett, B. O., “Pulse-burst PIV of an impulsively started cylinder in a shock tube for  $Re > 105$ ,” *Experiments in Fluids*, Vol. 59, No. 6, May 2018, pp. 106. doi: [10.1007/s00348-018-2558-4](https://doi.org/10.1007/s00348-018-2558-4).
- <sup>56</sup>Haertig, J., Havermann, M., Rey, C., and George, A., “Particle Image Velocimetry in Mach 3.5 and 4.5 Shock-Tunnel Flows,” *AIAA Journal*, Vol. 40, No. 6, 2002, pp. 1056–1060. doi: [10.2514/2.1787](https://doi.org/10.2514/2.1787).
- <sup>57</sup>Havermann, M., Haertig, J., Rey, C., and George, A., *PIV Measurements in Shock Tunnels and Shock Tubes*, Springer Berlin Heidelberg, Berlin, Heidelberg, 2008, pp. 429–443. doi: [10.1007/978-3-540-73528-1\\_23](https://doi.org/10.1007/978-3-540-73528-1_23).
- <sup>58</sup>Parker, R. A., Wakeman, T., MacLean, M., and Holden, M., “Measuring Nitric Oxide Freestream Velocity Using a Quantum Cascade Laser at CUBRC,” *Proceedings of 45th AIAA Aerospace Sciences Meeting and Exhibit*, AIAA-2007-1329, Kissimmee, Florida, 2007. doi: [10.2514/6.2007-1329](https://doi.org/10.2514/6.2007-1329).
- <sup>59</sup>Danehy, P. M., O’Byrne, S., Houwing, A. F. P., Fox, J. S., and Smith, D. R., “Flow-tagging Velocimetry for Hypersonic Flows using Fluorescence of Nitric Oxide,” *AIAA Journal*, Vol. 41, No. 2, 2003, pp. 263–271. doi: [10.2514/2.1939](https://doi.org/10.2514/2.1939).
- <sup>60</sup>de S. Matos, P. A., Barreta, L. G., and Martins, C. A., “Velocity and NO-Lifetime Measurements in an Unseeded Hypersonic Air Flow,” *Journal of Fluids Engineering*, Vol. 140, No. 12, 2018, pp. 121105. doi: [10.1115/1.4039863](https://doi.org/10.1115/1.4039863).
- <sup>61</sup>Hornung, H. G., “Performance Data of the New Free-Piston Shock Tunnel at GALCIT,” *Proceedings of 17th AIAA Aerospace Ground Testing Conference*, AIAA 1992-3943, Nashville, TN, 1992. doi: [10.2514/6.1992-3943](https://doi.org/10.2514/6.1992-3943).
- <sup>62</sup>Mills, J. L., Suenik, C. I., and Balla, R. J., “Hypersonic Wake Diagnostics Using Laser Induced Fluorescence Techniques,” *Proceedings of 42nd AIAA Plasmadynamics and Lasers Conference*, AIAA 2011-3459, Honolulu, Hawaii, 2011. doi: [10.2514/6.2011-3459](https://doi.org/10.2514/6.2011-3459).
- <sup>63</sup>Balla, R. J. and Everhart, J. L., “Rayleigh Scattering Density Measurements, Cluster Theory, and Nucleation Calculations at Mach 10,” *AIAA Journal*, Vol. 50, No. 3, 2012, pp. 698–707. doi: [10.2514/1.J051334](https://doi.org/10.2514/1.J051334).
- <sup>64</sup>Shekhtman, D., Mustafa, M. A., and Parziale, N. J., “Excitation Line Optimization for Krypton Tagging Velocimetry and Planar Laser-Induced Fluorescence in the 200-220 nm Rangei,” *Proceedings of AIAA Scitech 2021*, Virtual Event, 2021.
- <sup>65</sup>Miller, J. C., “Two-photon resonant multiphoton ionization and stimulated emission in krypton and xenon,” *Physical Review A*, Vol. 40, 1989, pp. 6969–6976. doi: [10.1103/PhysRevA.40.6969](https://doi.org/10.1103/PhysRevA.40.6969).
- <sup>66</sup>Shiu, Y. and Biondi, M. A., “Dissociative recombination in krypton: Dependence of the total rate coefficient and excited-state production on electron temperature,” *Physical Review Applied*, Vol. 16, Nov 1977, pp. 1817–1820. doi: [10.1103/PhysRevA.16.1817](https://doi.org/10.1103/PhysRevA.16.1817).
- <sup>67</sup>Dakka, M. A., Tsiminis, G., Glover, R. D., Perrella, C., Moffatt, J., Spooner, N. A., Sang, R. T., Light, P. S., and Luiten, A. N., “Laser-Based Metastable Krypton Generation,” *Phys. Rev. Lett.*, Vol. 121, Aug 2018, pp. 093201. doi: [10.1103/PhysRevLett.121.093201](https://doi.org/10.1103/PhysRevLett.121.093201).
- <sup>68</sup>Goodwin, D. G., “An Open-Source, Extensible Software Suite for CVD Process Simulation,” *Proceedings of CVD XVI and EuroCVD Fourteen, M Allendorf, F Maury, and F Teyssandier (Eds.)*, 2003, pp. 155–162.
- <sup>69</sup>Browne, S., Ziegler, J., and Shepherd, J. E., “Numerical Solution Methods for Shock and Detonation Jump Conditions,” GALCIT - FM2006-006, 2006.
- <sup>70</sup>Gordon, S. and McBride, B., “Thermodynamic Data to 20000 K for Monatomic Gases,” NASA TP-1999-208523, 1999.
- <sup>71</sup>McBride, B. J., Zehe, M. J., and Gordon, S., “NASA Glenn Coefficients for Calculating Thermodynamic Properties of Individual Species,” NASA TP-2002-211556, 2002.
- <sup>72</sup>Wright, M. J., Candler, G. V., and Prampolini, M., “Data-parallel Lower-upper Relaxation Method for the Navier-Stokes Equations,” *AIAA Journal*, Vol. 34, No. 7, 1996, pp. 1371–1377. doi: [10.2514/3.13242](https://doi.org/10.2514/3.13242).
- <sup>73</sup>Candler, G. V., “Hypersonic Nozzle Analysis Using an Excluded Volume Equation of State,” *Proceedings of 38th AIAA Thermophysics Conference*, AIAA-2005-5202, Toronto, Ontario Canada, 2005. doi: [10.2514/6.2005-5202](https://doi.org/10.2514/6.2005-5202).
- <sup>74</sup>Johnson, H. B., *Thermochemical Interactions in Hypersonic Boundary Layer Stability*, Ph.D. thesis, University of Minnesota, Minneapolis, Minnesota, 2000.
- <sup>75</sup>Wagnild, R. M., *High Enthalpy Effects on Two Boundary Layer Disturbances in Supersonic and Hypersonic Flow*, Ph.D. thesis, University of Minnesota, Minnesota, 2012.
- <sup>76</sup>Bélanger, J., *Studies of Mixing and Combustion in Hypervelocity Flows with Hot Hydrogen Injection*, Ph.D. thesis, California Institute of Technology, California, 1993.
- <sup>77</sup>O’Haver, T., *A Pragmatic Introduction to Signal Processing*, University of Maryland at College Park, 1997.
- <sup>78</sup>Bathel, B. F., Danehy, P. M., Inman, J. A., Jones, S. B., Ivey, C. B., and Goynes, C. P., “Velocity Profile Measurements in Hypersonic Flows Using Sequentially Imaged Fluorescence-Based Molecular Tagging,” *AIAA Journal*, Vol. 49, No. 9, 2011, pp. 1883–1896. doi: [10.2514/1.J050722](https://doi.org/10.2514/1.J050722).
- <sup>79</sup>Hill, R. B. and Klewicki, J. C., “Data reduction methods for flow tagging velocity measurements,” *Experiments in Fluids*, Vol. 20, No. 3, 1996, pp. 142–152. doi: [10.1007/BF00190270](https://doi.org/10.1007/BF00190270).